Am J Transl Res 2022;14(5):3037-3051
www.ajtr.org /ISSN:1943-8141/AJTR0141652

Original Article

Immune signatures of CD4 and CD68 predicts disease progression in cutaneous T cell lymphoma

Sanling Huang[1], Mengying Liao[2], Siliang Chen[1], Ping Zhang[1], Fangzhou Xu[1,3], Hongyu Zhang[1,3]

[1]Department of Hematology, Peking University Shenzhen Hospital, Shenzhen 518000, Guangdong, P. R. China; [2]Department of Pathology, Peking University Shenzhen Hospital, Shenzhen 518000, Guangdong, P. R. China; [3]The Clinical Trail Institute, Peking University Shenzhen Hospital, Shenzhen 518000, Guangdong, P. R. China

Received January 10, 2021; Accepted April 12, 2022; Epub May 15, 2022; Published May 30, 2022

Abstract: Background: Cutaneous T-cell lymphoma (CTCL) is highly heterogeneous, and its prognosis is closely related to the disease stage. The tumor microenvironment (TME) is an important component of tumor tissue, driving cancer cell growth, progression, and metastasis. However, the diagnostic value of TME in CTCL has not yet been studied in-depth. To date, no study has performed a comprehensive evaluation of the significance of the TME in CTCL. Methods: Using xCell methods based on bulk RNA sequencing data, we inferred immune cell fraction in the TME in 126 patients and assessed the prognostic importance of immune cells. Consensus clustering was performed to determine the TME subtypes and characterize the transcriptome of each subtype. Based on the TME subtypes, we established the disease progression model using random forest algorithms and logistic regression. The efficacy of the model was examined using an additional 49-patient cohort. Finally, we validated our finding at the protein level using immunochemistry in a 16-patient cohort. Results: Patients with advanced CTCL presented with a more active immunity overall than those with early stage. Random forest algorithms revealed that the immune cells CD4, macrophages, and dendritic cells (DCs) were the most effective prognosis predictors. Therefore, we constructed a risk model using logistic regression based on these immune cells. The TME score could be used to effectively predict disease conditions in three datasets with the AUC of 0.9414, 0.7912, and 0.7665, respectively. Immunochemistry at the protein level revealed that helper T cells and the macrophage markers CD4 and CD68 could successfully distinguish different CTCL stages in patients, whereas the DC marker langerin showed no change with disease progression. Conclusion: We found advanced-stage CTCL was associated with an active immune microenvironment, and the immune signatures CD4 and CD68 showed a relatively high accuracy in predicting CTCL disease progression.

Keywords: Cutaneous T-cell lymphoma, tumor microenvironment, macrophages, CD4, CD68

Introduction

Cutaneous T cell lymphoma (CTCL) is a non-Hodgkin lymphoma characterized by malignant $CD4^+$ T cell infiltration in the skin. The clinical prognosis varies greatly among patients with some presenting with a chronic and indolent condition, while for a small percentage it can be aggressive and fatal [1]. Furthermore, the stage of CTCL has a decisive influence on the prognosis of patients. Most patients with early-stage CTCL have a lengthy life expectancy; however, the survival rate reduces dramatically as the disease progresses [2]. Those with advanced illness (commonly referred to as Stage IIB or above) usually have a life expectancy of fewer than 5 years, whereas patients with early-stage disease (i.e., Stage IIA and lower) have a life expectancy of more than 15 years [3]. In addition, patients are advised to follow a personalized treatment plan depending on their clinical stage. Patients with early-stage CTCL are normally treated with conventional and topical medicines; whereas those with advanced-stage CTCL are encouraged to participate in clinical trials and get systemic treatment as soon as possible [4]. As a result, predicting clinical outcome and selecting anappropriate treatment plan requires a comprehensive understanding of the disease progression.

The cancer immune microenvironment is important in the growth, invasion, and metastasis of CTCL. This malignancy is characterized by systematic immune dysfunction and skin infiltration by cutaneous lymphocyte antigen (CLA)-

positive lymphocytes [5]. Thus, the skin environment, comprising various immune cell subsets as well as their interaction with malignant T cells through chemokines and cytokines, plays a central role in the development and pathogenesis of CTCL. Infiltrating immune cells can exert anti-tumor immunity; however, as they interact with tumor cells, they can also provide a suitable environment for tumor growth and metastasis [6]. The infiltrated immune cell pattern in the tumor microenvironment (TME) reflects the tumor immune response and predicts therapeutic benefits, especially from immunotherapy. Immune checkpoint inhibitors such as PD-1-Ab have achieved ideal treatment efficacy in Hodgkin lymphoma [7], melanoma [8], and many solid tumors [9]. However, immunotherapy is not appropriate for all patients, as successful tumor cell depletion requires an active anti-tumor immune microenvironment [10-13]. An inhibitory immune milieu characterized by suppressed cell activity and cytotoxic cell exhaustion often leads to a low immunotherapy response. The TME also affects the response of patients to conventional therapies like chemotherapy and radiotherapy [14]. Thus, identification of TME features facilitates the development of prognostic models and guides targeted therapy. Previous research has shown that the TME is an excellent predictor of prognosis and treatment response in solid tumors and B cell lymphoma [15-17]. Nevertheless, little is known about how the immunological state affects the clinical outcome of T cell lymphoma. Although the current CLIPi and CLIC score are the most widely used predictive tools for CTCL clinical risk [18-20], they ignore lymphoma microenvironments and cannot guide immunotherapy.

In this study, we first established a tool to predict risk of disease progression based on skin immune microenvironment features. By showing the expression of immune signatures, the TME score can help make decisions on treatment strategies, especially on immunotherapy.

Materials and methods

Data collection

The clinical information and RNA-sequencing (RNA-seq) data were obtained from the GEO database (https://www.ncbi.nlm.nih.gov/geo/). The keywords “cutaneous T cell lymphoma”, “mycosis fungoides”, and “gene expression/profiling” were used for searching. Datasets satisfying the following criteria were included: (1) skin samples from patients with primary CTCL and (2) availability of clinical information. The two largest datasets GSE70328 and GSE9479 were used for analysis. The mRNA-seq data were produced using the Affymetrix GeneChip HT-HG_U133A Early Access Array Platform and were processed using the Robust Multi-Chip Average. The third-largest dataset GSE113113, among those satisfying the inclusion criteria, was used for validation.

Immune cell type fraction analysis

We used the ssGSEA algorithm to calculate the pro- and anti-tumor immune infiltration scores (biomarkers are shown in Supplementary Table 1). Then, the webtool xCell was used to estimate the abundance of immune and stromal cell infiltration [21]. xCell integrates gene enrichment analysis with a deconvolution method and infers cell types based on the gene signature from RNA-seq or microarray data. The gene expression data were prepared following instructions by the developers and then uploaded to the xCell web portal (https://xcell.ucsf.edu/). From the 64 estimated cell types, we finally included 33 immune cell types (involved in innate and adaptive immunity) for further analysis.

Consensus clustering of TME-infiltrating cells

According to the xCell results, samples could be divided into different TME subgroups based on certain immune cell patterns. The *ConsensusClusterPlus* R package was applied to determine the number of clusters in the training cohort [22].

Identification of differentially expressed genes (DEGs)

The DEGs between the TME subgroups were identified using the R package *limma*. DEGs with an adjusted *P*-value <0.05 were considered for future analysis. For immune-related genes, the 4,872 reference genes were downloaded from the MSigDB database c7.all.v7.4.symbols (http://www.gsea-msigdb.org).

Gene ontology (GO) and gene set enrichment analysis (GSEA)

GO analysis and GSEA of DEGs were used for further functional enrichment analysis. GO

functional analyses were performed using the *enrichplot* and *clusterProfiler* R packages. Adjusted and unadjusted *P*-values <0.05 were considered significant. GSEA were performed using the software GSEA_4.1.0. A normalized enrichment score (NES) >1 and nominal *P*-value (NOM *P*-value) <0.05 were considered significant.

Model construction

The training cohort was made up of 89 randomly generated samples from the GSE70328 and GSE9479 datasets. The 37 remaining samples from the two datasets were used as test samples. Another CTCL dataset GSE113113 was used as the external validation cohort. Boosted classification trees and random forest, which were built with the *gbm* (v2.1.3) and *randomforest* R packages using log TPM values, were used to select immune cell signatures from the xCell data. Boosting was performed with 2,000 classification trees with a multinomial distribution. The algorithm was trained by shrinking class centroids toward the overall centroid or by a threshold amount that minimized the misclassification error as determined through 10-fold cross-validation on the training cohort. The variable importance of each cell type was assessed by quantifying the mean decrease in the Gini index of each predictor averaged overall splits. The cross-validation analysis showed that the misclassification error was the smallest when 6 variables were taken into consideration (Supplementary Figure 1). Then a classification model was constructed using Logistic regression with the *MASS* R package. The formula used was as follows:

$$\text{TME score} = \frac{\exp(\beta_0 + \beta_1 x_1 + \beta_2 x_2 + \cdots + \beta_n x_n)}{1 + \exp(\beta_0 + \beta_1 x_1 + \beta_2 x_2 + \cdots + \beta_n x_n)}$$

Whereby patients with a TME score over 0.5 were classified into a clinical high risk of disease progression group. To test the accuracy of the disease progression model, the receiver operating characteristic (ROC) curve analysis was performed using the *pROC* R package.

Immunohistochemistry (IHC) validation

To identify the malignant cells, macrophages, and dendritic cells (DCs), IHC was performed. The skin samples were collected from Peking University, Shenzhen Hospital, from 2005 to 2020. The clinical features of patients are summarized in Supplementary Table 1. For antigen retrieval, the slides from formalin-fixed paraffin-embedded CTCL tissue specimens were heat-treated by boiling in EDTA Antigen Retrieval Solution (pH 8.0; Solarbio, Beijing, China) for 20 min. Then, the sections were blocked with BSA solution for 20 min at 25°C. To detect CD4, CD68, and langerin levels, the slides were incubated with monoclonal antibody (Abcam, Cambridge, UK) at 1:200 dilution (overnight at 4°C); the IHC Kit for Mouse Primary Antibody (ZSGB-Bio, Beijing, China) was used as secondary antibody and then stained with 3,3'-diaminobenzidine reagents according to manufacturer's instructions. Each incubation step was followed by three 5 min washes in PBS buffer. Hematoxylin-eosin (H&E) staining was used to investigate the overall immune state and was conducted according to procedures in published articles [23].

The staining results were semi-quantified by a pathologist (Liao) using the following system. Stain color scores (at 100× magnification): no staining, 0; pale yellow, 1; tan, 2; brown, 3; and the final stain color score was taken as the average of five different microscopic fields. Stain color proportion (at 40× magnification): no staining in any cells, 0; staining in less than 25% of cells, 1; staining in 25-50% of cells, 1; staining in 50-75% of cells, 3; staining in more than 75% of cells, 4; The final result of IHC score was calculated by multiplying stain color scores and stain color proportions.

Statistical analysis

All statistical analyses were performed using the software R version 4.1.1 (The R Foundation for Statistical Computing, MO, USA) by *Student's t test*. Adjusted *P*-values <0.05 were considered significant.

Results

Landscape of TME cells in CTCL

The study consisted of 175 specimens, including 126 patients in the training cohort (GSE70328, *n*=63, and GSE9479, *n*=63) and 49 in the validation cohort (GSE113113). The study design is shown as a flowchart in **Figure 1**. To analyze the immune landscape in the TME in CTCL, we used the ssGSEA algorithm to

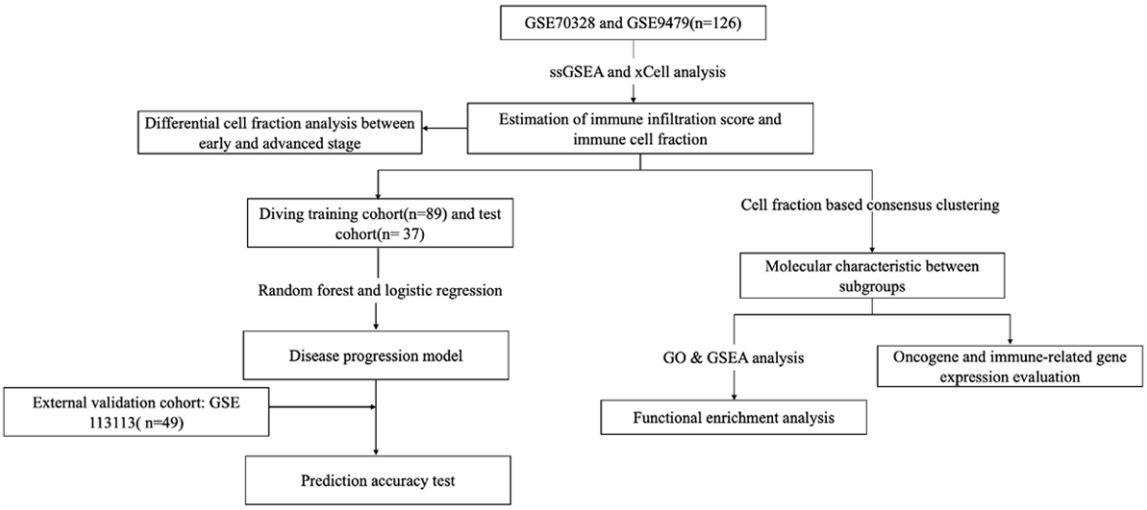

Figure 1. Flow chart of comprehensive analysis of tumor microenvironment in cutaneous T cell lymphoma.

infer a tumor-related immune cell infiltration score based on bulk tumor expression data. According to immune cell markers (Supplementary Table 2), the fraction of both anti-tumor and pro-tumor immune cells was calculated. As shown in **Figure 2A**, cells showing anti-tumor activity (e.g., activated $CD8^+$ cells, type 1 helper cells) and suppressive pro-tumor activity (e.g., type 2 helper cells, regulatory T cells) were positively correlated according to the Pearson's correlation test. Compared to patients with early-stage CTCL, those with advanced-stage were characterized by a rich abundance of anti-tumor immunity (P=0.0076) and had more active pro-tumor activity (P=0.015) (**Figure 2B** and **2C**).

Next, we portrayed the immune cell pattern using the xCell algorithm. We correlated the immune cell landscape with the clinical stage (**Figure 2D**) which showed that many innate immune cells that were decreased as the disease progressed, including DCs, eosinophils, and NK T cells, while neutrophils, as well as M1 and M2 macrophages, showed an increased proportion in patients with advanced-stage CTCL. For adaptive immunity, many T lymphocyte subtypes increased in the advanced stage, such as CD4 memory T cells, CD8 central memory T cells, and CD8 effector memory T cells. However, the B lymphocytes did not seem to play an important role in CTCL - as they only consisted of a small fraction of immune cells with a minor difference between disease stages.

Identification of two TME subtypes of CTCL

Based on the heterogeneity of infiltrating immune cells in CTCL, we assessed potential clusters using the consensus clustering method and obtained two stable clusters termed clusters A and B. The TME in cluster B was distinguished by rich infiltration in most immune cells, whereas immune cell infiltration was poor in cluster A except for DCs (**Figure 3A**). Also, we noticed that the TME of patients in cluster B was mostly associated with advanced CTCL, indicating a positive correlation between an active TME and disease progression (**Figure 3B**). Cluster B also had a higher average expression of oncogenes. Most tumor-related gene signatures, like *KIR3DL3, TOX*, and *JUNB* were higher in cluster B, except for the T cell differentiation regulator *GATA3* (**Figure 3C**).

Afterward, we conducted DEG analysis on two TME subtypes to illustrate the underlying biological characteristics of different TME subtypes. We obtained 6,325 significant DEGs between the two TME subtypes (P<0.01), with the most upregulated genes in cluster A being immune-related genes that present antigens such as *FCER1A*, *HLA-DQB2*, *CD1C*, *CD1E*, and *CD207* (**Figure 4A**). In cluster B, the most significantly upregulated genes were cell proliferation-related genes like *SAMD9* and *AIM2*. The GSEA indicated that genes involved in *MYC*, *mTOR*, and *E2F* pathways showed statistically significant upregulation in TME cluster B (**Figure**

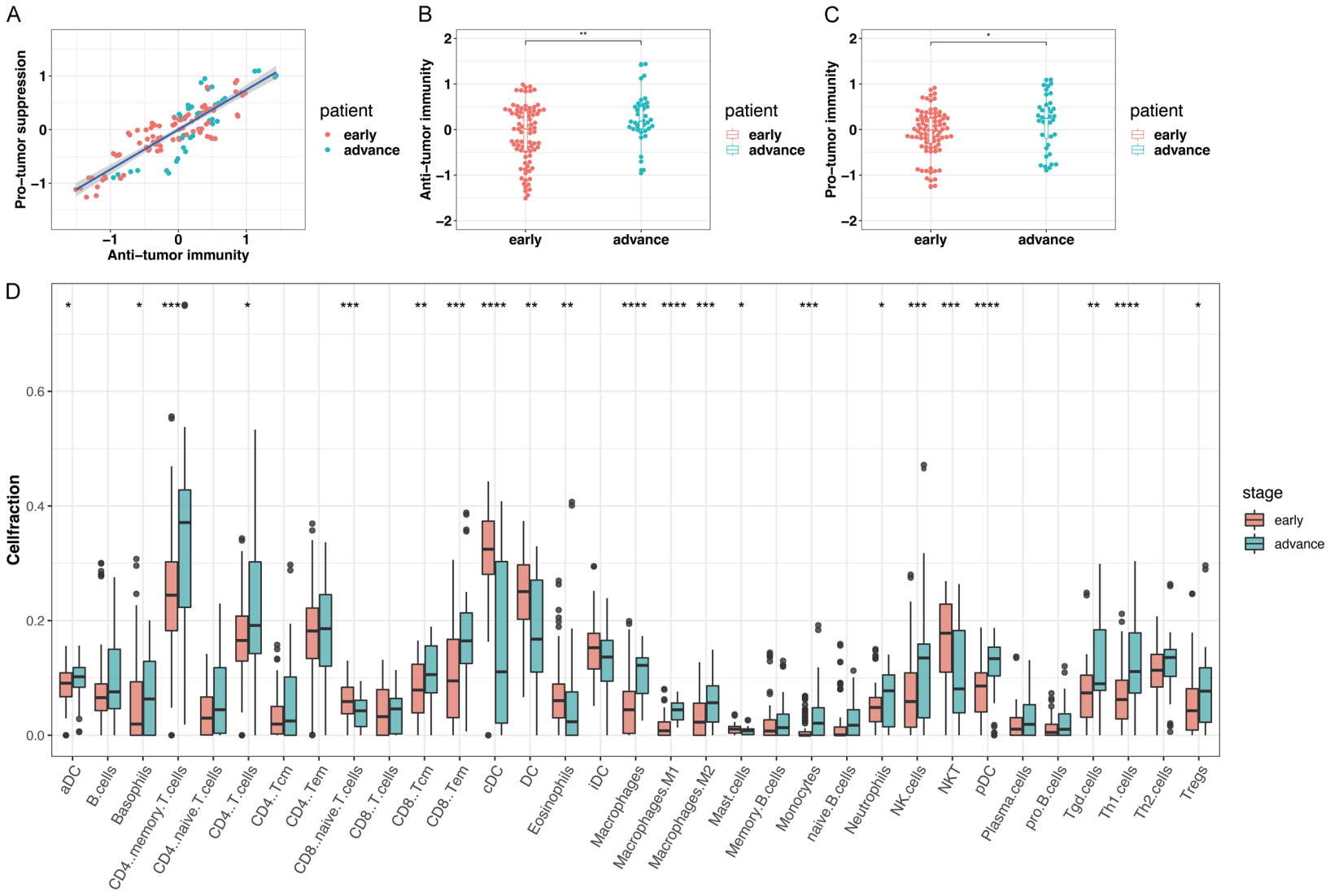

Figure 2. Estimation of immune infiltration score and immune cell fraction. A. Correlation between infiltration of cell types executing anti-tumor immunity and pro-tumor, immune-suppressive functions. The shaded area represents a 95% confidence interval. B, C. Correlation between clinical stage of patients as well as their anti- and pro-tumor immunity. D. Immune cell abundance in different stages of CTCL in patients. *P* values obtained using Student's *t*-test. **P*<0.05, ***P*<0.01, ****P*<0.001, *****P*<0.0001.

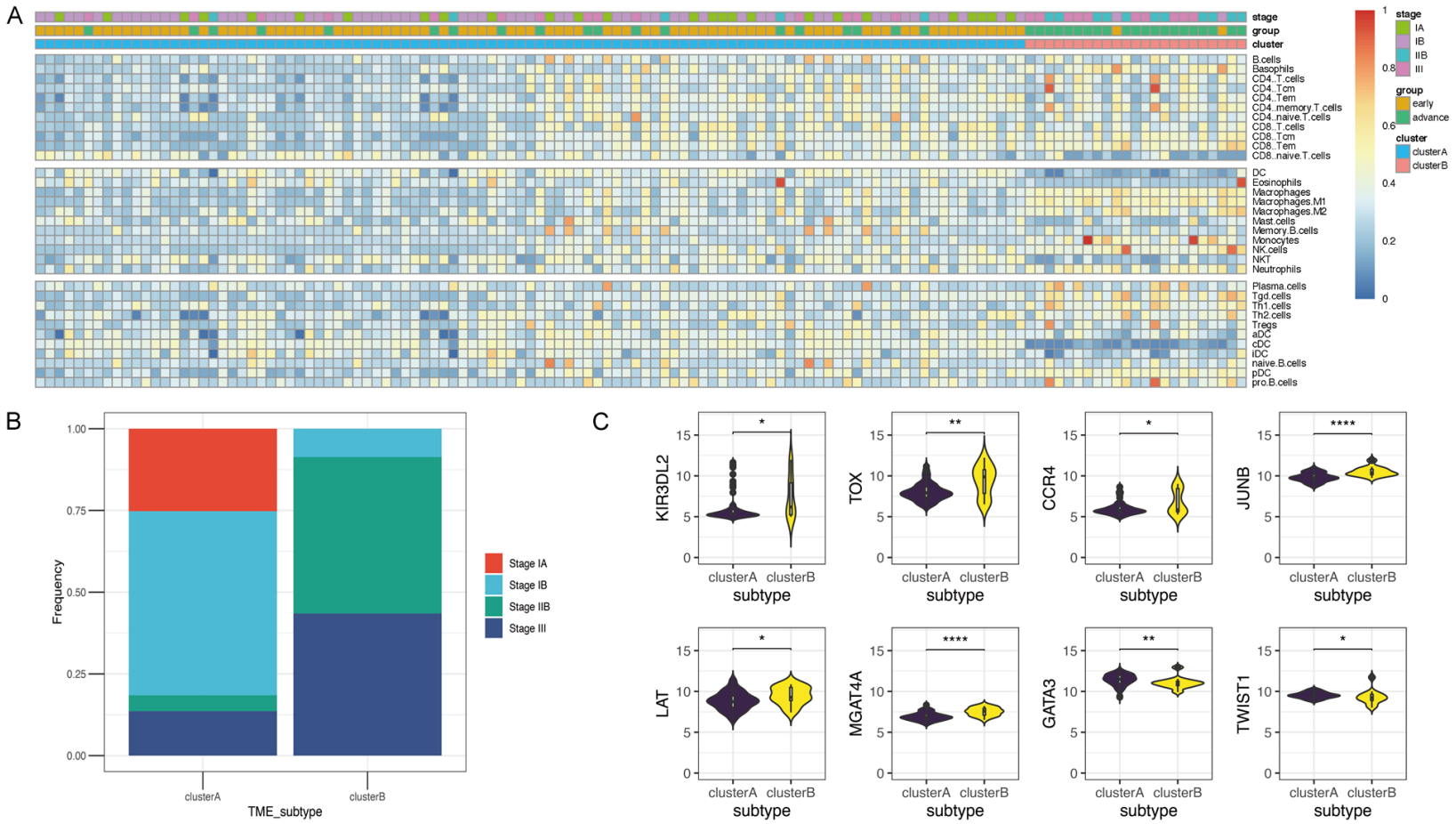

Figure 3. Identification of two TME subtypes in CTCL. A. TME immune cell fraction in 126 patients. B. Correlation between TME subtypes and clinical TNMB stage of patients. C. Expression of CTCL oncogenes in two TME subtypes. The y-axis shows the $\log_2$ TPM of each gene. *P* values obtained using Student's *t*-test. **P*<0.05, ***P*<0.01, ****P*<0.001, *****P*<0.0001.

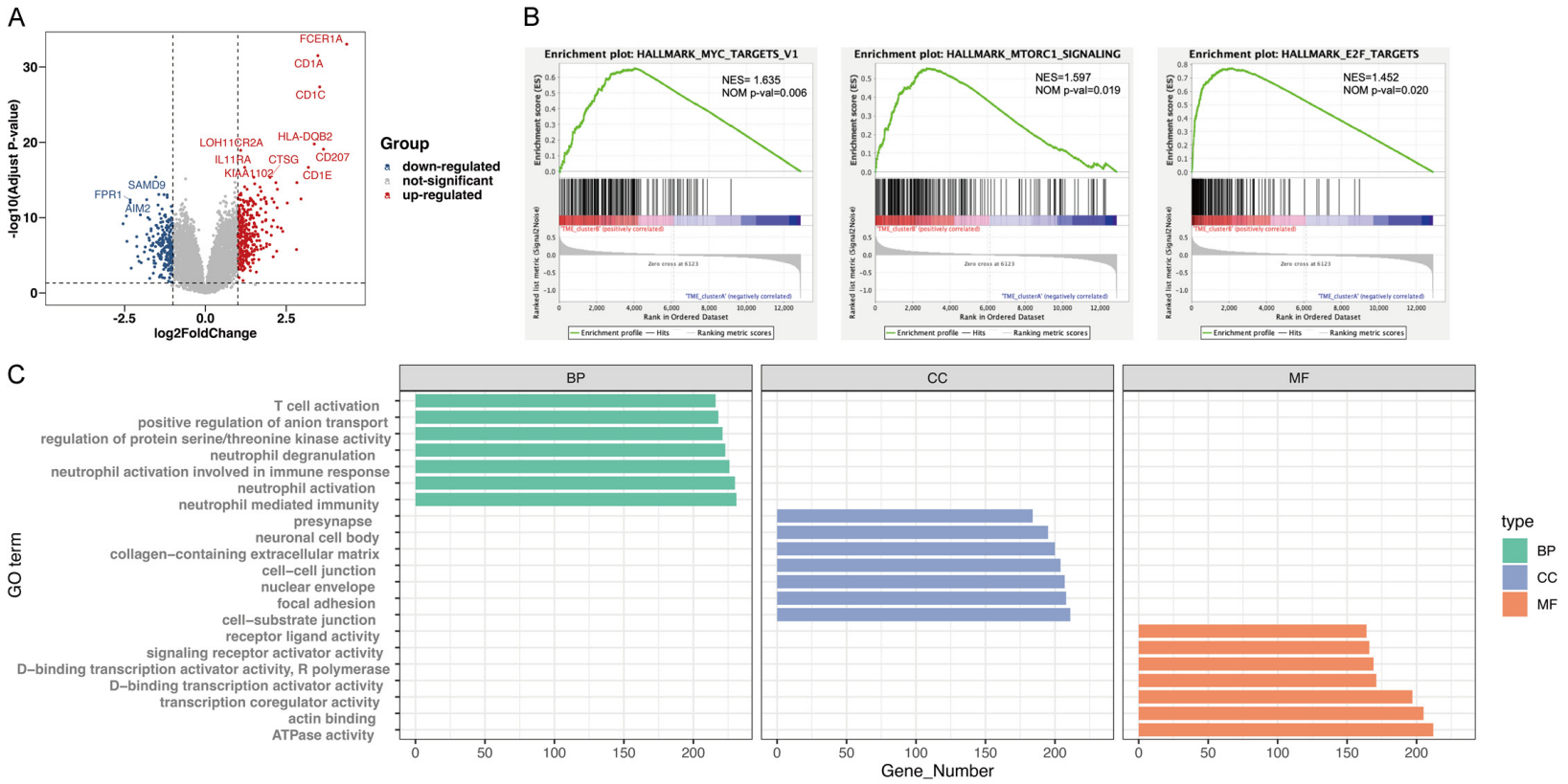

Figure 4. Molecular features of two TME subtypes. A. Differentially expressed genes in TME clusters A vs B. The red dots indicate genes upregulated in cluster A with $\log_2$ Fold-Change >1 and adjusted P<0.05. The blue dots indicate genes downregulated in cluster A with $\log_2$ Fold Change >1 and adjusted P<0.05. The grey dots indicate no significant change. B. The GSEA enrichment of differentially expressed genes. The normalized enrichment score (NES) >1 and nominal *P*-value (NOM *P*-value) <0.05 were considered significant. C. Gene ontology (GO) enrichment of the upregulated genes in cluster B. The x-axis denotes the number of genes within each GO term. BP: Biologic process; CC: Cellular component; MF: Molecular function.

4B). GO analysis indicated substantial enrichment of genes involved in neutrophil-related immune response, small molecular metabolism, and ATPase activity (**Figure 4C**).

Immune state of the 2 TME subtypes

To further investigate the immune status of the two distinct TME subtypes, we analyzed the expression of 104 immune-related genes (**Figure 5A**). The overall expression of immune-related genes was not significantly different between the two subtypes, but genes regulating cytotoxicity and immune checkpoints had a higher expression in TME cluster B. Moreover, we analyzed the expression patterns of immune checkpoint genes (**Figure 5B**). The results showed that almost all immune checkpoints were significantly overexpressed in TME cluster B compared to TME cluster A except for *PDCD1*, *ICOS*, and *GITR*.

TME score predicted clinical stage in CTCL

To apply the TME classification practically, we constructed the TME score using random forest and logistic regression algorithms based on immune cell types to represent the features of the TME clusters. The study population included 89 patients in the training cohort (randomly generated from GSE 70328 and GSE 9479), and 86 in the test cohort (37 from the GSE70328 and GSE 9479 datasets, 49 patients from GSE113113). Using random forest, the phenotype signatures were extracted from the 33 immune infiltrating cells through dimensionality reduction. Among all immune cells, six cell types were considered important for predicting clinical stage, including macrophages, M1 macrophages, DCs, conventional DCs (cDC), $CD4^+$ T cells, and $CD4^+$ memory cells (Supplementary Figure 1C). Besides the tumor cells, the antigen presenting cells were most important in determining disease progression. Next, we constructed a logistic regression model with the following formula:

$$\text{TME score} = \frac{\exp(1.18 + 0.76 \times CD4 + memory\ T\ cells - 2.32 \times CD4 + T\ cells + 12.94 \times cDC - 13.62 \times DC + 60.74 \times Macrophages - 195.75 \times M1\ Macrophages)}{1 + \exp(1.18 + 0.76 \times CD4 + memory\ T\ cells - 2.32 \times CD4 + T\ cells + 12.94 \times cDC - 13.62 \times DC + 60.74 \times Macrophages - 195.75 \times \text{M1}\ Macrophages)}$$

and found a significantly higher TME score in cluster A vs cluster B. Then we evaluated the test cohort and one independent dataset GSE113113. The TME score showed high diagnostic value in both the training and test cohort (area under the curve [AUC]=0.9414 in the training cohort, AUC=0.7912 in the test cohort, and AUC=0.7665 in the external validation cohort GSE113113) (**Figure 6A-C**). To test the diagnostic value of our model at the protein level, we performed IHC staining of CD4, CD68, and langerin in 16 CTCL skin samples. In patients with advanced CTCL, the average infiltration IHC scores of CD4 cells and TAMs were higher than that of patients with early stage (P=0.096 and P=0.21, respectively) (**Figure 6D**). However, unexpectedly, the IHC score for DC infiltration was equally low in both stages with less than 25% DC infiltration in most patients. **Figure 6E-H** exhibit the HE and IHC staining image of patient 12, who suffered from IVA-stage MF, and **Figure 6I-L** exhibit the HE and IHC staining image of patient 9, who was stage IB MF when the skin biopsy sample was collected. While the density and intensity of $CD4^+$ and $CD68^+$ cells were significantly higher in patient 12, there was no significant difference of Langerin between the two different stage patients.

Discussion

CTCL arises from malignant T lymphocyte clones in the skin, accompanied by chronic inflammation in the cancer lesion. Furthermore, as the disease progress, the tumor cells start to circulate between skin, lymph nodes, and peripheral blood. CTCL comprises two major subtypes, MF and SS, together constituting more than half of all cases [24]. Mycosis fungoides (MF), often recognized as early-stage Sezary Syndrome (SS), is slowly progressive and characterized by limited patches and plaques in the photo-protected skin. With a TNMB stage under IV, the average life expectancy of patients with MF can be up to 15 years. On the contrary, SS, the leukemic form of MF, is aggressive and lethal. Patients present with erythroderma and a high burden of malignant T cells (called Sezary cells) in the blood (1,000 cells/μL). Once diagnosed with SS, patients suffer a rapid progressive course and have an average life expectancy of less than 2 years [25].

The skin microenvironment plays a central role in the development and progression of CTCL.

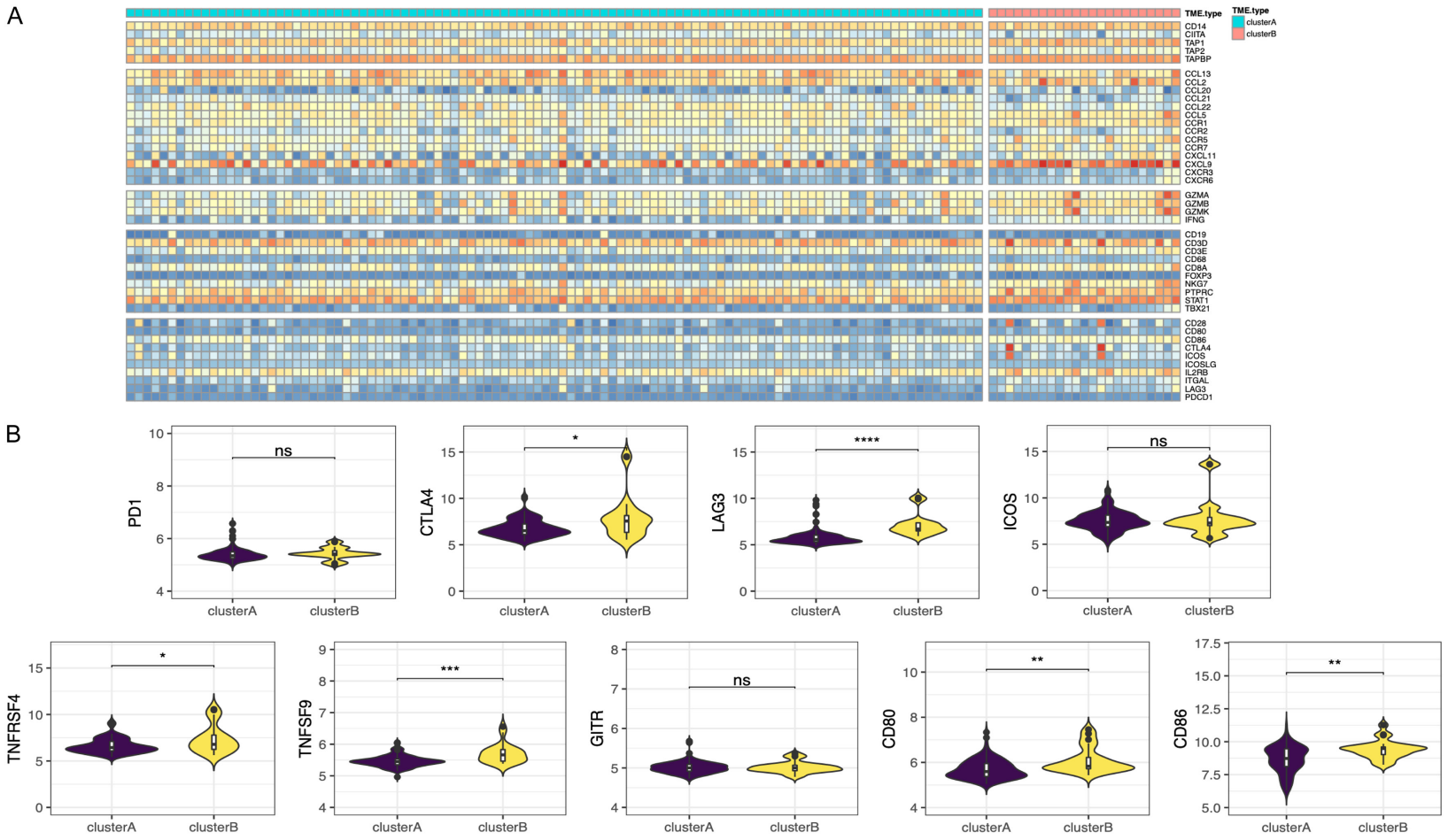

Figure 5. Immune gene signatures of two TME subtypes. A. The expression of immune genes in two TME subtypes. B. Immune checkpoint expression in the two TME subtypes. The y-axis shows the $\log_2$ TPM of each gene. *P* values obtained using Student's *t*-test. **P*<0.05, ***P*<0.01, ****P*<0.001, *****P*<0.0001.

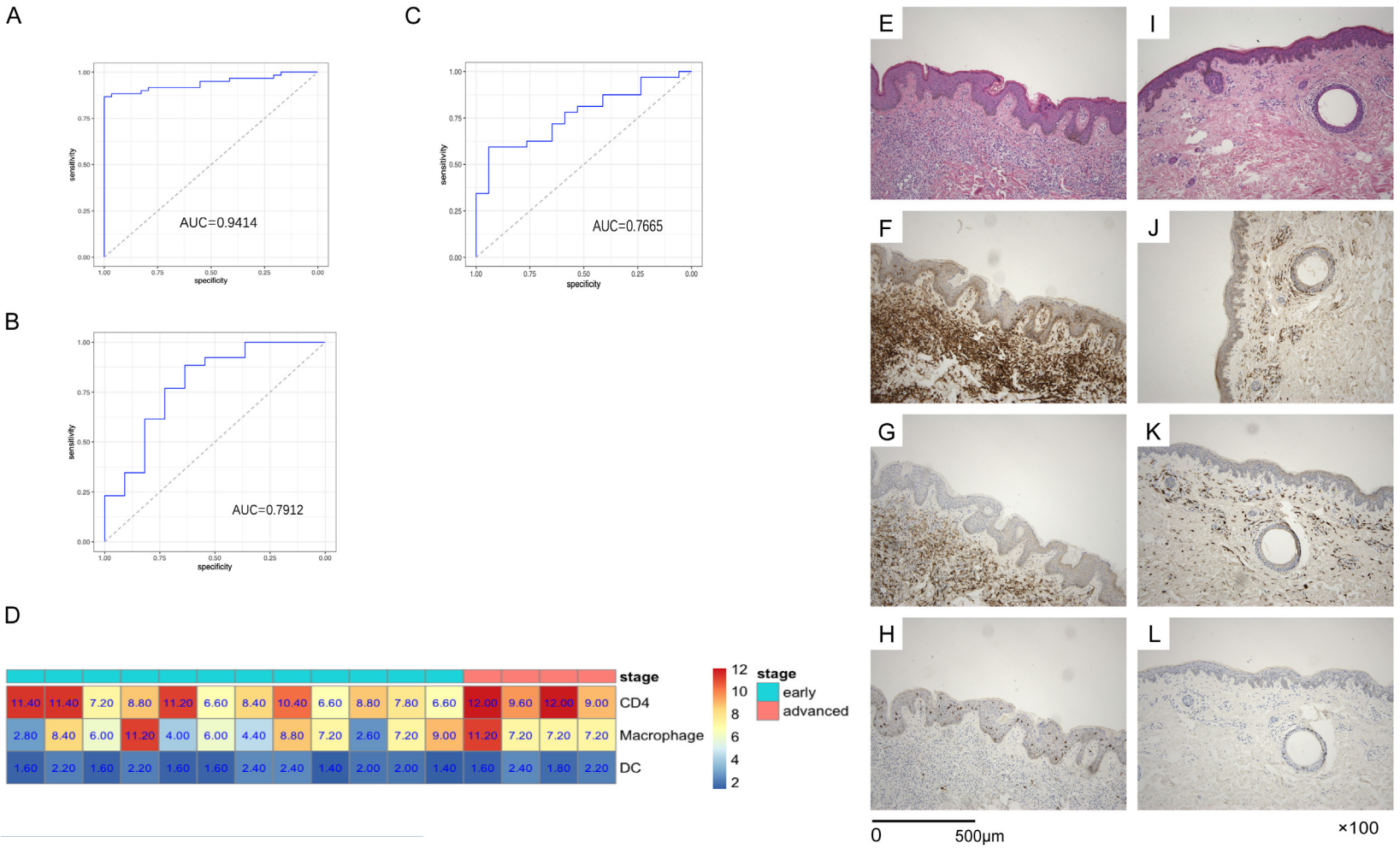

Figure 6. Diagnostic value of the TME model. A-C. The receiver operating characteristic (ROC) curve of test cohort, internal validation cohort, and external validation cohort (GSE 113113). D. The immunohistochemistry (IHC) score of CD4, CD68, and langerin in the cohort with 16 patients. The staining results were semi-quantified by a pathologist using the following system. Stain color scores (at 100× magnification): No staining, 0; Pale yellow, 1; Tan, 2; Brown, 3; and the final stain color score was taken as the average of five different microscopic fields. Stain color proportion (at 40× magnification): No staining in any cells, 0; Staining in less than 25% of cells, 1; Staining in 25-50% of cells, 1; Staining in 50-75% of cells, 3; Staining in more than 75% of cells, 4. The final result or IHC score was calculated by combining multiple stain color scores and stain color proportions. E-H. The hematoxylin-eosin (H&E) as well as CD4-, CD68-, and langerin-staining of a patient with advanced CTCL. All staining figures are shown at a magnification of ×100 (Scale Bar: 500 μm). I-L. The H&E as well as CD4-, CD68-, and langerin-staining of a patient with early-stage CTCL. All staining figures are shown at a magnification of ×100. (Scale Bar: 500 μm).

Recent studies have demonstrated that the tumor immune milieu (i.e., tumor cells, tumor-infiltrating T cells, macrophages, DCs, mast cells) with their interactions as well as secreted chemokines and cytokines are crucial for malignant clone proliferation and escape from immunosurveillance [10, 13]. Our study revealed that CTCL is a heterogeneous disease on the TME level with disease progression accompanied by immune activation. Unlike B cell lymphoma or solid tumors [16, 17, 26], most patients with advanced stage had a relatively hot TME, shown by rich infiltration of both cells exerting cytotoxic and prohibitory ability. We next analyzed the correlation between immune cell patterns and the clinicopathologic features of patients. Apart from the tumor cells, the most significant differences between patients with early and advanced-stage CTCL were innate immune cells such as dendritic cells, macrophages, NK, and NKT cells. In accordance with a previous study, although the difference was not significant during either early (stage I to stage IIA)- or advanced (stage IIB to stage IV)-disease in patients, the conventional DC depletion and pDC recruitment in the skin were strongly observed in patients at tumor stage (IV) as compared to other stages (stage I to stage III) [27]. Another antigen presentating-related cell subtype, the macrophage, had an upwards trend in patients with advanced-stage CTCL [28, 29]. Both studies indicated the importance of antigen presentation and stimulation in the progression of CTCL. Surprisingly, we found that the increase in NK cell number correlated with poor prognosis, which may be explained by the hypothesis set forth by Mundy-Bosse et al.: impaired NK cell recognition functions and their increased number resulted from high levels of IL-15 secreted by malignant $CD4^+$ cells [30]. The role of innate immunity was undoubtedly crucial in both immune surveillance and immune escape in CTCL.

As for the specific acquired immunity, B cells and $CD8^+$ T cells did not seem to differ between early- and advanced-stage CTCL. Our study suggests that B cells had almost no significant correlation with tumor stage in CTCL. The function of B cells can vary in different types of cancers [31-33] but they mostly play an active role in anti-tumor immunity. Although the tumor clones were type 2 helper T cells, most patients had reduced humoral immunity which needs further investigation in CTCL. As for $CD8^+$ T cells, although the total number of $CD8^+$ cells did not increase according to the disease stage, the $CD8^+$ memory cells exhibited a higher percentage in patients with stage IIB or higher. Torrealba et al. found a likely phenomenon in the peripheral blood of patients with SS [34]: compared to healthy controls, although patients with SS had reduced numbers of total $CD8^+$ T cells, they exhibited higher percentages of effector and memory cells, indicating a chronic activation of CD8 cells. Overall, the advanced patients usually had a higher fraction of macrophages, effector or memory CD8 cells, less infiltration of DC, NK, and eosinophils, and showed no significant difference in B cells. The immune cell infiltration patterns were largely shaped by the clinical features.

Next, to show how certain immune cell infiltration patterns determine the transcriptome feature of patients, we used a consensus clustering algorithm to identify potential TME subtypes in CTCL. Patients were divided into two TME clusters: cluster A represented a less abundant infiltration of immune cells than its counterparts, while cluster B exhibited a more advanced stage than A with a higher overall expression of oncogenes including *KIR3DL3*, *TOX*, and *JUNB*. Therefore, we hypothesized that increased cancer cells could drive the activation of neighboring immune cells and guide them to downregulate immunosurveillance through chronic activation. Compared to TME cluster A, the major downregulated genes were antigen-presentation genes with upregulated genes in cell proliferation in TME cluster B, which was consistent with our finding that DC cells decreased in patients during late-stage CTCL. GSEA further proved this finding, as the most enriched DEGs were components of the *mTOR*, *MYC*, and *E2F* pathway demonstrating a positive association between an active immune microenvironment and tumor cell proliferation ability. Subsequently, we examined the expression of immune-related genes to demonstrate the functional differences between the two groups. Results suggested that the chemokine profile was not significantly different between immune active and immune repressed conditions. The C-C and C-X-C motif chemokines were secreted from both malignant T cells as well as infiltrated

immune cells [35] - serving as coordinators of immune cell movement. Two TME subtypes expressed similar chemokines, suggesting the signal exchanges in the tumor milieu were as active in different immune states. Molecules that indicated cytotoxic abilities and immune checkpoints showed greater expression in TME cluster B, indicating that patients with advanced stage had a strong anti-tumor immunity and upregulation of inhibitory signals. We especially focused on immune checkpoints, and though intriguingly most immune checkpoints were overexpressed in the immune active subgroup, the expression of *PDCD1* showed no significant difference between groups. This was consistent with recent findings [36, 37], and the role of PD-1 may be complex as *in vivo* models have shown it can also be a haploinsufficient suppressor of malignant T cells [38]. In addition, we found that the T cell and NK cell activator *LAG3* was the most upregulated gene in the TME active subcluster, indicating a potential clinical application of LAG3 inhibitor to restore T cell function from exhaustion.

Finally, we constructed a disease progression prediction model to classify patients into different groups. Using the results of the inferred cell fraction, the model successfully predicted the clinical stage in different datasets. To test whether our results could be used in pathological diagnosis, we conducted an IHC experiment. Our cohort with 16 patients validated the effectiveness of CD4 and CD68 when deciding progression risk; however, the marker of mature DC cells, langerin, did not show a meaningful difference between groups.

There are limitations in our study. First, the sizes of included RNA-sequencing cases and IHC cases were small, and this was due to the overall incidence of CTCL was rather low and it was hard for single center studies to enroll many qualified patients. Second, although the xCell algorithm enabled us to infer fractions of immune cell subsets, the precise state was masked by bulk genomic methods; for example, we were not able to know the expression of exhausted markers on $CD8^+$ T cells. Lastly, single cell RNA sequencing has been introduced to the research on CTCL as a powerful approach which provides deep insight into cell-to-cell variation in both tumor and microenvironment. Thus, single cell RNA sequencing is likely to help us gain a more comprehensive and profound understanding of tumor microenvironment in CTCL. Overall, more genomic analyses, especially at the single cell level, from different medical centers are needed to establish better understanding of tumor microenvironment in CTCL.

Conclusions

We comprehensively analyzed the immune cell landscape of TME in patients with CTCL and correlated the clinicopathologic features of patients with RNA sequencing data available online. Based on immune cell patterns, we identified two molecularly distinct CTCL types with different immune patterns and tumor burdens. According to our findings, we believe that our classification system of CTCL might contribute to predicting the clinical outcomeof patients and guide physicians when prescribing immune checkpoint inhibitors.

Acknowledgements

We would like to thank Xiaoming Yin from the pathology department of Shenzhen Hospital for his instruction in immunochemistry experiments.

Disclosure of conflict of interest

None.

Address correspondence to: Hongyu Zhang, Department of Hematology, Peking University Shenzhen Hospital, No. 1120 Lianhua Road, Shenzhen 518000, Guangdong, P. R. China. E-mail: 1911210753@bjmu.edu.cn

References

[1] Dummer R, Vermeer MH, Scarisbrick JJ, Kim YH, Stonesifer C, Tensen CP, Geskin LJ, Quaglino P and Ramelyte E. Cutaneous T cell lymphoma. Nat Rev Dis Primers 2021; 7: 61.

[2] Farabi B, Seminario-Vidal L, Jamgochian M, Akay BN, Atak MF, Rao BK, Karagaiah P, Grabbe S and Goldust M. Updated review on prognostic factors in mycosis fungoides and new skin lymphoma trials. J Cosmet Dermatol 2021; [Epub ahead of print].

[3] Quaglino P, Fava P, Pileri A, Grandi V, Sanlorenzo M, Panasiti V, Guglielmo A, Alberti-Violetti S, Novelli M, Astrua C, Rubatto M, Tonella L, Berti E, Pimpinelli N, Osella Abate S, Fierro MT, Ver-

meer M, Scarisbrick JJ and Ribero S. phenotypical markers, molecular mutations, and immune microenvironment as targets for new treatments in patients with mycosis fungoides and/or sézary syndrome. J Invest Dermatol 2021; 141: 484-495.

[4] Hristov AC, Tejasvi T and A Wilcox R. Cutaneous T-cell lymphomas: 2021 update on diagnosis, risk-stratification, and management. Am J Hematol 2021; 96: 1313-1328.

[5] Borowitz MJ, Weidner A, Olsen EA and Picker LJ. Abnormalities of circulating T-cell subpopulations in patients with cutaneous T-cell lymphoma: cutaneous lymphocyte-associated antigen expression on T cells correlates with extent of disease. Leukemia 1993; 7: 859-863.

[6] Quail DF and Joyce JA. Microenvironmental regulation of tumor progression and metastasis. Nat Med 2013; 19: 1423-1437.

[7] Shi Y, Su H, Song Y, Jiang W, Sun X, Qian W, Zhang W, Gao Y, Jin Z, Zhou J, Jin C, Zou L, Qiu L, Li W, Yang J, Hou M, Zeng S, Zhang Q, Hu J, Zhou H, Xiong Y and Liu P. Safety and activity of sintilimab in patients with relapsed or refractory classical Hodgkin lymphoma (ORIENT-1): a multicentre, single-arm, phase 2 trial. Lancet Haematol 2019; 6: e12-e19.

[8] Hamid O, Robert C, Daud A, Hodi FS, Hwu WJ, Kefford R, Wolchok JD, Hersey P, Joseph RW, Weber JS, Dronca R, Gangadhar TC, Patnaik A, Zarour H, Joshua AM, Gergich K, Elassaiss-Schaap J, Algazi A, Mateus C, Boasberg P, Tumeh PC, Chmielowski B, Ebbinghaus SW, Li XN, Kang SP and Ribas A. Safety and tumor responses with lambrolizumab (anti-PD-1) in melanoma. N Engl J Med 2013; 369: 134-144.

[9] Topalian SL, Hodi FS, Brahmer JR, Gettinger SN, Smith DC, McDermott DF, Powderly JD, Carvajal RD, Sosman JA, Atkins MB, Leming PD, Spigel DR, Antonia SJ, Horn L, Drake CG, Pardoll DM, Chen L, Sharfman WH, Anders RA, Taube JM, McMiller TL, Xu H, Korman AJ, Jure-Kunkel M, Agrawal S, McDonald D, Kollia GD, Gupta A, Wigginton JM and Sznol M. Safety, activity, and immune correlates of anti-PD-1 antibody in cancer. N Engl J Med 2012; 366: 2443-2454.

[10] Bruni D, Angell HK and Galon J. The immune contexture and Immunoscore in cancer prognosis and therapeutic efficacy. Nat Rev Cancer 2020; 20: 662-680.

[11] Kumagai S, Togashi Y, Kamada T, Sugiyama E, Nishinakamura H, Takeuchi Y, Vitaly K, Itahashi K, Maeda Y, Matsui S, Shibahara T, Yamashita Y, Irie T, Tsuge A, Fukuoka S, Kawazoe A, Udagawa H, Kirita K, Aokage K, Ishii G, Kuwata T, Nakama K, Kawazu M, Ueno T, Yamazaki N, Goto K, Tsuboi M, Mano H, Doi T, Shitara K and Nishikawa H. The PD-1 expression balance between effector and regulatory T cells predicts the clinical efficacy of PD-1 blockade therapies. Nat Immunol 2020; 21: 1346-1358.

[12] Galon J and Bruni D. Approaches to treat immune hot, altered and cold tumours with combination immunotherapies. Nat Rev Drug Discov 2019; 18: 197-218.

[13] Galon J, Mlecnik B, Bindea G, Angell HK, Berger A, Lagorce C, Lugli A, Zlobec I, Hartmann A, Bifulco C, Nagtegaal ID, Palmqvist R, Masucci GV, Botti G, Tatangelo F, Delrio P, Maio M, Laghi L, Grizzi F, Asslaber M, D'Arrigo C, Vidal-Vanaclocha F, Zavadova E, Chouchane L, Ohashi PS, Hafezi-Bakhtiari S, Wouters BG, Roehrl M, Nguyen L, Kawakami Y, Hazama S, Okuno K, Ogino S, Gibbs P, Waring P, Sato N, Torigoe T, Itoh K, Patel PS, Shukla SN, Wang Y, Kopetz S, Sinicrope FA, Scripcariu V, Ascierto PA, Marincola FM, Fox BA and Pagès F. Towards the introduction of the 'Immunoscore' in the classification of malignant tumours. J Pathol 2014; 232: 199-209.

[14] Hirata E and Sahai E. Tumor microenvironment and differential responses to therapy. Cold Spring Harb Perspect Med 2017; 7: a026781.

[15] Van den Eynde M, Mlecnik B, Bindea G, Fredriksen T, Church SE, Lafontaine L, Haicheur N, Marliot F, Angelova M, Vasaturo A, Bruni D, Jouret-Mourin A, Baldin P, Huyghe N, Haustermans K, Debucquoy A, Van Cutsem E, Gigot JF, Hubert C, Kartheuser A, Remue C, Léonard D, Valge-Archer V, Pagès F, Machiels JP and Galon J. The link between the multiverse of immune microenvironments in metastases and the survival of colorectal cancer patients. Cancer Cell 2018; 34: 1012-1026.

[16] Ma SY, Tian XP, Cai J, Su N, Fang Y, Zhang YC, Wang JN, Peter Gale R and Cai QQ. A prognostic immune risk score for diffuse large B-cell lymphoma. Br J Haematol 2021; 194: 111-119.

[17] Huang J, Li J, Zheng S, Lu Z, Che Y, Mao S, Lei Y, Zang R, Liu C, Wang X, Fang L, Sun N and He J. Tumor microenvironment characterization identifies two lung adenocarcinoma subtypes with specific immune and metabolic state. Cancer Sci 2020; 111: 1876-1886.

[18] Benton EC, Crichton S, Talpur R, Agar NS, Fields PA, Wedgeworth E, Mitchell TJ, Cox M, Ferreira S, Liu P, Robson A, Calonje E, Stefanato CM, Wilkins B, Scarisbrick J, Wain EM, Child F, Morris S, Duvic M and Whittaker SJ. A cutaneous lymphoma international prognostic index (CLIPi) for mycosis fungoides and sezary syndrome. Eur J Cancer 2013; 49: 2859-2868.

[19] Danish HH, Liu S, Jhaveri J, Flowers CR, Lechowicz MJ, Esiashvili N and Khan MK. Validation

of cutaneous lymphoma international prognostic index (CLIPI) for mycosis fungoides and Sézary syndrome. Leuk Lymphoma 2016; 57: 2813-2819.

[20] Scarisbrick JJ, Prince HM, Vermeer MH, Quaglino P, Horwitz S, Porcu P, Stadler R, Wood GS, Beylot-Barry M, Pham-Ledard A, Foss F, Girardi M, Bagot M, Michel L, Battistella M, Guitart J, Kuzel TM, Martinez-Escala ME, Estrach T, Papadavid E, Antoniou C, Rigopoulos D, Nikolaou V, Sugaya M, Miyagaki T, Gniadecki R, Sanches JA, Cury-Martins J, Miyashiro D, Servitje O, Muniesa C, Berti E, Onida F, Corti L, Hodak E, Amitay-Laish I, Ortiz-Romero PL, Rodríguez-Peralto JL, Knobler R, Porkert S, Bauer W, Pimpinelli N, Grandi V, Cowan R, Rook A, Kim E, Pileri A, Patrizi A, Pujol RM, Wong H, Tyler K, Stranzenbach R, Querfeld C, Fava P, Maule M, Willemze R, Evison F, Morris S, Twigger R, Talpur R, Kim J, Ognibene G, Li S, Tavallaee M, Hoppe RT, Duvic M, Whittaker SJ and Kim YH. Cutaneous lymphoma international consortium study of outcome in advanced stages of mycosis fungoides and sézary syndrome: effect of specific prognostic markers on survival and development of a prognostic model. J Clin Oncol 2015; 33: 3766-3773.

[21] Aran D, Hu Z and Butte AJ. xCell: digitally portraying the tissue cellular heterogeneity landscape. Genome Biol 2017; 18: 220.

[22] Wilkerson MD and Hayes DN. ConsensusClusterPlus: a class discovery tool with confidence assessments and item tracking. Bioinformatics 2010; 26: 1572-1573.

[23] Onodera Y, Shimizu H, Yamashita S, Nishikawa T and Nishikawa T. Cryofixed, freeze-dried and paraffin-embedded skin enables successful immunohistochemical staining of skin basement membrane antigens. Histochemistry 1992; 98: 87-91.

[24] Jawed SI, Myskowski PL, Horwitz S, Moskowitz A and Querfeld C. Primary cutaneous T-cell lymphoma (mycosis fungoides and Sézary syndrome): part I. Diagnosis: clinical and histopathologic features and new molecular and biologic markers. J Am Acad Dermatol 2014; 70: 205.

[25] Child F and Whittaker S. Primary cutaneous T-cell lymphoma. J Am Acad Dermatol 2014; 264-282.

[26] Shou Y, Yang L, Yang Y, Zhu X, Li F and Xu J. Determination of hypoxia signature to predict prognosis and the tumor immune microenvironment in melanoma. Mol Omics 2021; 17: 307-316.

[27] Pileri A, Agostinelli C, Sessa M, Quaglino P, Santucci M, Tomasini C, Grandi V, Fava P, Astrua C, Righi S, Patrizi A, Pileri SA and Pimpinelli N. Langerhans, plasmacytoid dendritic and myeloid-derived suppressor cell levels in mycosis fungoides vary according to the stage of the disease. Virchows Arch 2017; 470: 575-582.

[28] Sugaya M, Miyagaki T, Ohmatsu H, Suga H, Kai H, Kamata M, Fujita H, Asano Y, Tada Y, Kadono T, Okochi H and Sato S. Association of the numbers of CD163(+) cells in lesional skin and serum levels of soluble CD163 with disease progression of cutaneous T cell lymphoma. J Dermatol Sci 2012; 68: 45-51.

[29] Furudate S, Fujimura T, Kakizaki A, Kambayashi Y, Asano M, Watabe A and Aiba S. The possible interaction between periostin expressed by cancer stroma and tumor-associated macrophages in developing mycosis fungoides. Exp Dermatol 2016; 25: 107-112.

[30] Mundy-Bosse B, Denlinger N, McLaughlin E, Chakravarti N, Hwang S, Chen L, Mao HC, Kline D, Youssef Y, Kohnken R, Lee DA, Lozanski G, Freud AG, Porcu P, William B, Caligiuri MA and Mishra A. Highly cytotoxic natural killer cells are associated with poor prognosis in patients with cutaneous T-cell lymphoma. Blood Adv 2018; 2: 1818-1827.

[31] Lundgren S, Berntsson J, Nodin B, Micke P and Jirström K. Prognostic impact of tumour-associated B cells and plasma cells in epithelial ovarian cancer. J Ovarian Res 2016; 9: 21.

[32] Mehdipour F, Razmkhah M, Faghih Z, Bagheri M, Talei AR and Ghaderi A. The significance of cytokine-producing B cells in breast tumor-draining lymph nodes. Cell Oncol (Dordr) 2019; 42: 381-395.

[33] Berntsson J, Nodin B, Eberhard J, Micke P and Jirström K. Prognostic impact of tumour-infiltrating B cells and plasma cells in colorectal cancer. Int J Cancer 2016; 139: 1129-1139.

[34] Torrealba MP, Manfrere KC, Miyashiro DR, Lima JF, de MOL, Pereira NZ, Cury-Martins J, Pereira J, Duarte AJS, Sato MN and Sanches JA. Chronic activation profile of circulating CD8+ T cells in Sézary syndrome. Oncotarget 2018; 9: 3497-3506.

[35] Patil K, Kuttikrishnan S, Khan AQ, Ahmad F, Alam M, Buddenkotte J, Ahmad A, Steinhoff M and Uddin S. Molecular pathogenesis of cutaneous T cell lymphoma: role of chemokines, cytokines, and dysregulated signaling pathways. Semin Cancer Biol 2021; [Epub ahead of print].

[36] Vergnolle I, Douat-Beyries C, Boulinguez S, Rieu JB, Vial JP, Baracou R, Boudot S, Cazeneuve A, Chaugne S, Durand M, Estival S, Lablanche N, Nicolau-Travers ML, Tournier E, Lamant L and Vergez F. CD158k and PD-1 expressions define heterogeneous subtypes of Sezary syndrome. Blood Adv 2022; 6: 1813-1825.

[37] Park J, Daniels J, Wartewig T, Ringbloom KG, Martinez-Escala ME, Choi S, Thomas JJ, Doukas PG, Yang J, Snowden C, Law C, Lee Y, Lee K, Zhang Y, Conran C, Tegtmeyer K, Mo SH, Pease DR, Jothishankar B, Kwok PY, Abdulla FR, Pro B, Louissaint A, Boggon TJ, Sosman J, Guitart J, Rao D, Ruland J and Choi J. Integrated genomic analyses of cutaneous T-cell lymphomas reveal the molecular bases for disease heterogeneity. Blood 2021; 138: 1225-1236.

[38] Wartewig T, Kurgyis Z, Keppler S, Pechloff K, Hameister E, Öllinger R, Maresch R, Buch T, Steiger K, Winter C, Rad R and Ruland J. PD-1 is a haploinsufficient suppressor of T cell lymphomagenesis. Nature 2017; 552: 121-125.

Supplementary Table 1. The clinical information of 16 patients who provided skin samples for IHC validation

ID	Sex	Age	clinical stage
1	Male	68	IVA
2	Female	47	IB
3	Male	35	IA
4	Male	29	IB
5	Female	37	IVA
6	Male	78	IIA
7	Female	45	IIA
8	Male	50	III
9	Male	47	IB
10	Female	68	IIA
11	Male	32	IA
12	Male	49	IVA
13	Male	81	IIA
14	Male	46	IB
15	Male	82	IB
16	Male	38	IIA

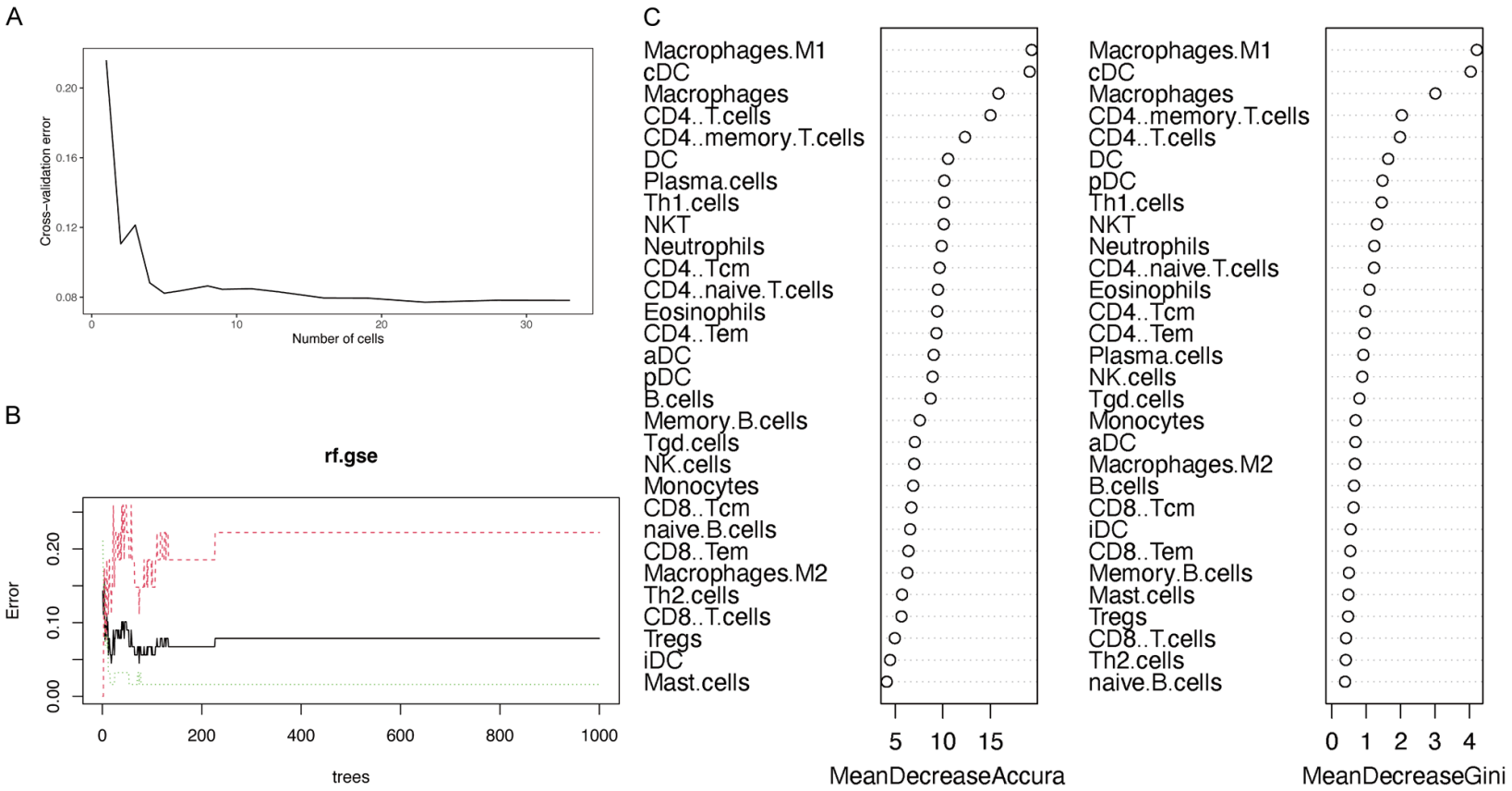

Supplementary Figure 1. Choice of important variance in the disease progression model. A, B. Using cross-validation algorithm to decide the number of random forest trees and variance. For 200 trees and 6 variances, the cross-validation error is the smallest. C. The six most important factors that influence disease stage in patients.

Supplementary Table 2. Gene signatures used for calculating GSEA immune score

Metagene	Cell type	Immunity	Metagene	Cell type	Immunity
ADAM28	Activated B cell	Anti-tumor	GPR44	Type 17 T helper cell	Anti-tumor
CD180	Activated B cell	Anti-tumor	IFT80	Type 17 T helper cell	Anti-tumor
CD79B	Activated B cell	Anti-tumor	ASB2	Type 2 T helper cell	Pro-tumor
BLK	Activated B cell	Anti-tumor	CSRP2	Type 2 T helper cell	Pro-tumor
CD19	Activated B cell	Anti-tumor	DAPK1	Type 2 T helper cell	Pro-tumor
MS4A1	Activated B cell	Anti-tumor	DLC1	Type 2 T helper cell	Pro-tumor
TNFRSF17	Activated B cell	Anti-tumor	DNAJC12	Type 2 T helper cell	Pro-tumor
IGHM	Activated B cell	Anti-tumor	DUSP6	Type 2 T helper cell	Pro-tumor
GNG7	Activated B cell	Anti-tumor	GNAI1	Type 2 T helper cell	Pro-tumor
MICAL3	Activated B cell	Anti-tumor	LAMP3	Type 2 T helper cell	Pro-tumor
SPIB	Activated B cell	Anti-tumor	NRP2	Type 2 T helper cell	Pro-tumor
HLA-DOB	Activated B cell	Anti-tumor	OSBPL1A	Type 2 T helper cell	Pro-tumor
IGKC	Activated B cell	Anti-tumor	PDE4B	Type 2 T helper cell	Pro-tumor
PNOC	Activated B cell	Anti-tumor	PHLDA1	Type 2 T helper cell	Pro-tumor
FCRL2	Activated B cell	Anti-tumor	PLA2G4A	Type 2 T helper cell	Pro-tumor
BACH2	Activated B cell	Anti-tumor	RAB27B	Type 2 T helper cell	Pro-tumor
CR2	Activated B cell	Anti-tumor	RBMS3	Type 2 T helper cell	Pro-tumor
TCL1A	Activated B cell	Anti-tumor	RNF125	Type 2 T helper cell	Pro-tumor
AKNA	Activated B cell	Anti-tumor	TMPRSS3	Type 2 T helper cell	Pro-tumor
ARHGAP25	Activated B cell	Anti-tumor	GATA3	Type 2 T helper cell	Pro-tumor
CCL21	Activated B cell	Anti-tumor	BIRC5	Type 2 T helper cell	Pro-tumor
CD27	Activated B cell	Anti-tumor	CDC25C	Type 2 T helper cell	Pro-tumor
CD38	Activated B cell	Anti-tumor	CDC7	Type 2 T helper cell	Pro-tumor
CLEC17A	Activated B cell	Anti-tumor	CENPF	Type 2 T helper cell	Pro-tumor
CLEC9A	Activated B cell	Anti-tumor	CXCR6	Type 2 T helper cell	Pro-tumor
CLECL1	Activated B cell	Anti-tumor	DHFR	Type 2 T helper cell	Pro-tumor
ADRM1	Activated CD8 T cell	Anti-tumor	EVI5	Type 2 T helper cell	Pro-tumor
AHSA1	Activated CD8 T cell	Anti-tumor	GSTA4	Type 2 T helper cell	Pro-tumor
C1GALT1C1	Activated CD8 T cell	Anti-tumor	HELLS	Type 2 T helper cell	Pro-tumor
CCT6B	Activated CD8 T cell	Anti-tumor	IL26	Type 2 T helper cell	Pro-tumor
CD37	Activated CD8 T cell	Anti-tumor	LAIR2	Type 2 T helper cell	Pro-tumor
CD3D	Activated CD8 T cell	Anti-tumor	ABAT	CD56 bright natural killer cell	Anti-tumor
CD3E	Activated CD8 T cell	Anti-tumor	C11orf75	CD56 bright natural killer cell	Anti-tumor
CD3G	Activated CD8 T cell	Anti-tumor	C5orf15	CD56 bright natural killer cell	Anti-tumor
CD69	Activated CD8 T cell	Anti-tumor	CDHR1	CD56 bright natural killer cell	Anti-tumor
CD8A	Activated CD8 T cell	Anti-tumor	DCAF12	CD56 bright natural killer cell	Anti-tumor
CETN3	Activated CD8 T cell	Anti-tumor	DYNLL1	CD56 bright natural killer cell	Anti-tumor
CSE1L	Activated CD8 T cell	Anti-tumor	GPR137B	CD56 bright natural killer cell	Anti-tumor
GEMIN6	Activated CD8 T cell	Anti-tumor	HCP5	CD56 bright natural killer cell	Anti-tumor
GNLY	Activated CD8 T cell	Anti-tumor	HDGFRP2	CD56 bright natural killer cell	Anti-tumor
GPT2	Activated CD8 T cell	Anti-tumor	KRT86	CD56 bright natural killer cell	Anti-tumor
GZMA	Activated CD8 T cell	Anti-tumor	MLST8	CD56 bright natural killer cell	Anti-tumor
GZMH	Activated CD8 T cell	Anti-tumor	ELMOD3	CD56 bright natural killer cell	Anti-tumor
GZMK	Activated CD8 T cell	Anti-tumor	ENTPD5	CD56 bright natural killer cell	Anti-tumor
IL2RB	Activated CD8 T cell	Anti-tumor	FAM119A	CD56 bright natural killer cell	Anti-tumor
LCK	Activated CD8 T cell	Anti-tumor	FAM179A	CD56 bright natural killer cell	Anti-tumor
MPZL1	Activated CD8 T cell	Anti-tumor	CLIC2	CD56 bright natural killer cell	Anti-tumor

NKG7	Activated CD8 T cell	Anti-tumor	COX7A2L	CD56 bright natural killer cell	Anti-tumor
PIK3IP1	Activated CD8 T cell	Anti-tumor	CREB3L4	CD56 bright natural killer cell	Anti-tumor
PTRH2	Activated CD8 T cell	Anti-tumor	CSF1	CD56 bright natural killer cell	Anti-tumor
TIMM13	Activated CD8 T cell	Anti-tumor	CSNK2A2	CD56 bright natural killer cell	Anti-tumor
ZAP70	Activated CD8 T cell	Anti-tumor	CSTA	CD56 bright natural killer cell	Anti-tumor
ACTN4	Central memory CD8 T cell	Anti-tumor	CSTB	CD56 bright natural killer cell	Anti-tumor
ADAM12	Central memory CD8 T cell	Anti-tumor	CTPS	CD56 bright natural killer cell	Anti-tumor
ADCY9	Central memory CD8 T cell	Anti-tumor	CTSD	CD56 bright natural killer cell	Anti-tumor
F13A1	Central memory CD8 T cell	Anti-tumor	FST	CD56 bright natural killer cell	Anti-tumor
FCER1G	Central memory CD8 T cell	Anti-tumor	GATA2	CD56 bright natural killer cell	Anti-tumor
FCGR3B	Central memory CD8 T cell	Anti-tumor	GMPR	CD56 bright natural killer cell	Anti-tumor
FGF7	Central memory CD8 T cell	Anti-tumor	HDC	CD56 bright natural killer cell	Anti-tumor
FKBP4	Central memory CD8 T cell	Anti-tumor	HEY1	CD56 bright natural killer cell	Anti-tumor
GLUD1	Central memory CD8 T cell	Anti-tumor	HOXA1	CD56 bright natural killer cell	Anti-tumor
GM2A	Central memory CD8 T cell	Anti-tumor	HS2ST1	CD56 bright natural killer cell	Anti-tumor
GUSB	Central memory CD8 T cell	Anti-tumor	HS3ST1	CD56 bright natural killer cell	Anti-tumor
IL1RN	Central memory CD8 T cell	Anti-tumor	BCL11B	CD56 bright natural killer cell	Anti-tumor
NOL11	Central memory CD8 T cell	Anti-tumor	CDH3	CD56 bright natural killer cell	Anti-tumor
NTRK1	Central memory CD8 T cell	Anti-tumor	MYL6B	CD56 bright natural killer cell	Anti-tumor
RARA	Central memory CD8 T cell	Anti-tumor	NAA16	CD56 bright natural killer cell	Anti-tumor
RNF128	Central memory CD8 T cell	Anti-tumor	CIQA	CD56 bright natural killer cell	Anti-tumor
SIGLEC1	Central memory CD8 T cell	Anti-tumor	CIQB	CD56 bright natural killer cell	Anti-tumor
TNFRSF11A	Central memory CD8 T cell	Anti-tumor	CYP27B1	CD56 bright natural killer cell	Anti-tumor
TOX4	Central memory CD8 T cell	Anti-tumor	EIF3M	CD56 bright natural killer cell	Anti-tumor
UBA52	Central memory CD8 T cell	Anti-tumor	CYP27A1	CD56 dim natural killer cell	Pro-tumor
ULBP1	Central memory CD8 T cell	Anti-tumor	DDX55	CD56 dim natural killer cell	Pro-tumor
ACAP1	Effector memory CD8 T cell	Anti-tumor	DYRK2	CD56 dim natural killer cell	Pro-tumor
APOL3	Effector memory CD8 T cell	Anti-tumor	RPL37A	CD56 dim natural killer cell	Pro-tumor
ARHGAP10	Effector memory CD8 T cell	Anti-tumor	NOTCH3	CD56 dim natural killer cell	Pro-tumor
ATP10D	Effector memory CD8 T cell	Anti-tumor	AKR7A3	CD56 dim natural killer cell	Pro-tumor
C3AR1	Effector memory CD8 T cell	Anti-tumor	GPRC5C	CD56 dim natural killer cell	Pro-tumor
CCR5	Effector memory CD8 T cell	Anti-tumor	GRIN1	CD56 dim natural killer cell	Pro-tumor
CD160	Effector memory CD8 T cell	Anti-tumor	HLA-E	CD56 dim natural killer cell	Pro-tumor
CD55	Effector memory CD8 T cell	Anti-tumor	PORCN	CD56 dim natural killer cell	Pro-tumor
CFLAR	Effector memory CD8 T cell	Anti-tumor	PSMC4	CD56 dim natural killer cell	Pro-tumor
CMKLR1	Effector memory CD8 T cell	Anti-tumor	UPP1	CD56 dim natural killer cell	Pro-tumor
DAPP1	Effector memory CD8 T cell	Anti-tumor	IL21R	CD56 dim natural killer cell	Pro-tumor
FCRL6	Effector memory CD8 T cell	Anti-tumor	KIR2DS1	CD56 dim natural killer cell	Pro-tumor
FLT3LG	Effector memory CD8 T cell	Anti-tumor	KIR2DS2	CD56 dim natural killer cell	Pro-tumor
GZMM	Effector memory CD8 T cell	Anti-tumor	KIR2DS5	CD56 dim natural killer cell	Pro-tumor
HAPLN3	Effector memory CD8 T cell	Anti-tumor	ACADM	Immature dendritic cell	Pro-tumor
HLA-DMB	Effector memory CD8 T cell	Anti-tumor	AHCYL1	Immature dendritic cell	Pro-tumor
HLA-DPA1	Effector memory CD8 T cell	Anti-tumor	ALDH1A2	Immature dendritic cell	Pro-tumor
HLA-DPB1	Effector memory CD8 T cell	Anti-tumor	ALDH3A2	Immature dendritic cell	Pro-tumor
IFI16	Effector memory CD8 T cell	Anti-tumor	ALDH9A1	Immature dendritic cell	Pro-tumor
LIME1	Effector memory CD8 T cell	Anti-tumor	ALOX15	Immature dendritic cell	Pro-tumor
LTK	Effector memory CD8 T cell	Anti-tumor	AMT	Immature dendritic cell	Pro-tumor
NFKBIA	Effector memory CD8 T cell	Anti-tumor	ARL1	Immature dendritic cell	Pro-tumor
SETD7	Effector memory CD8 T cell	Anti-tumor	ATIC	Immature dendritic cell	Pro-tumor

SIK1	Effector memory CD8 T cell	Anti-tumor	ATP5A1	Immature dendritic cell	Pro-tumor
TRIB2	Effector memory CD8 T cell	Anti-tumor	CAPZA1	Immature dendritic cell	Pro-tumor
CCL3L1	Regulatory T cell	Pro-tumor	LILRA5	Immature dendritic cell	Pro-tumor
CD72	Regulatory T cell	Pro-tumor	RDX	Immature dendritic cell	Pro-tumor
CLEC5A	Regulatory T cell	Pro-tumor	RRAGD	Immature dendritic cell	Pro-tumor
FOXP3	Regulatory T cell	Pro-tumor	TACSTD2	Immature dendritic cell	Pro-tumor
ITGA4	Regulatory T cell	Pro-tumor	INPP5F	Immature dendritic cell	Pro-tumor
L1CAM	Regulatory T cell	Pro-tumor	RAB38	Immature dendritic cell	Pro-tumor
LIPA	Regulatory T cell	Pro-tumor	PLAU	Immature dendritic cell	Pro-tumor
LRP1	Regulatory T cell	Pro-tumor	CSF3R	Immature dendritic cell	Pro-tumor
LRRC42	Regulatory T cell	Pro-tumor	SLC18A2	Immature dendritic cell	Pro-tumor
MARCO	Regulatory T cell	Pro-tumor	AMPD2	Immature dendritic cell	Pro-tumor
MMP12	Regulatory T cell	Pro-tumor	CLTB	Immature dendritic cell	Pro-tumor
MNDA	Regulatory T cell	Pro-tumor	C1orf162	Immature dendritic cell	Pro-tumor
MRC1	Regulatory T cell	Pro-tumor	AIF1	Macrophage	Pro-tumor
MS4A6A	Regulatory T cell	Pro-tumor	CCL1	Macrophage	Pro-tumor
PELO	Regulatory T cell	Pro-tumor	CCL14	Macrophage	Pro-tumor
PLEK	Regulatory T cell	Pro-tumor	CCL23	Macrophage	Pro-tumor
PRSS23	Regulatory T cell	Pro-tumor	CCL26	Macrophage	Pro-tumor
PTGIR	Regulatory T cell	Pro-tumor	CD300LB	Macrophage	Pro-tumor
ST8SIA4	Regulatory T cell	Pro-tumor	CNR1	Macrophage	Pro-tumor
STAB1	Regulatory T cell	Pro-tumor	CNR2	Macrophage	Pro-tumor
CD70	Type 1 T helper cell	Anti-tumor	EIF1	Macrophage	Pro-tumor
TBX21	Type 1 T helper cell	Anti-tumor	EIF4A1	Macrophage	Pro-tumor
ADAM8	Type 1 T helper cell	Anti-tumor	FPR1	Macrophage	Pro-tumor
AHCYL2	Type 1 T helper cell	Anti-tumor	FPR2	Macrophage	Pro-tumor
ALCAM	Type 1 T helper cell	Anti-tumor	FRAT2	Macrophage	Pro-tumor
B3GALNT1	Type 1 T helper cell	Anti-tumor	GPR27	Macrophage	Pro-tumor
BBS12	Type 1 T helper cell	Anti-tumor	GPR77	Macrophage	Pro-tumor
BST1	Type 1 T helper cell	Anti-tumor	RNASE2	Macrophage	Pro-tumor
CD151	Type 1 T helper cell	Anti-tumor	MS4A2	Macrophage	Pro-tumor
CD47	Type 1 T helper cell	Anti-tumor	BASP1	Macrophage	Pro-tumor
CD48	Type 1 T helper cell	Anti-tumor	IGSF6	Macrophage	Pro-tumor
CD52	Type 1 T helper cell	Anti-tumor	HK3	Macrophage	Pro-tumor
CD53	Type 1 T helper cell	Anti-tumor	VNN1	Macrophage	Pro-tumor
CD59	Type 1 T helper cell	Anti-tumor	FES	Macrophage	Pro-tumor
CD6	Type 1 T helper cell	Anti-tumor	NPL	Macrophage	Pro-tumor
CD68	Type 1 T helper cell	Anti-tumor	FZD2	Macrophage	Pro-tumor
CD7	Type 1 T helper cell	Anti-tumor	FAM198B	Macrophage	Pro-tumor
CD96	Type 1 T helper cell	Anti-tumor	HNMT	Macrophage	Pro-tumor
CFHR3	Type 1 T helper cell	Anti-tumor	SLC15A3	Macrophage	Pro-tumor
CHRM3	Type 1 T helper cell	Anti-tumor	CD4	Macrophage	Pro-tumor
CLEC7A	Type 1 T helper cell	Anti-tumor	TXNDC3	Macrophage	Pro-tumor
COL23A1	Type 1 T helper cell	Anti-tumor	FRMD4A	Macrophage	Pro-tumor
COL4A4	Type 1 T helper cell	Anti-tumor	CRYBB1	Macrophage	Pro-tumor
COL5A3	Type 1 T helper cell	Anti-tumor	HRH1	Macrophage	Pro-tumor
DAB1	Type 1 T helper cell	Anti-tumor	WNT5B	Macrophage	Pro-tumor
DLEU7	Type 1 T helper cell	Anti-tumor	CD101	Natural killer T cell	Anti-tumor
DOC2B	Type 1 T helper cell	Anti-tumor	CD109	Natural killer T cell	Anti-tumor

EMP1	Type 1 T helper cell	Anti-tumor	CNPY3	Natural killer T cell	Anti-tumor
F12	Type 1 T helper cell	Anti-tumor	CNPY4	Natural killer T cell	Anti-tumor
FURIN	Type 1 T helper cell	Anti-tumor	CREB1	Natural killer T cell	Anti-tumor
GAB3	Type 1 T helper cell	Anti-tumor	CRTC2	Natural killer T cell	Anti-tumor
GATM	Type 1 T helper cell	Anti-tumor	CRTC3	Natural killer T cell	Anti-tumor
GFPT2	Type 1 T helper cell	Anti-tumor	CSF2	Natural killer T cell	Anti-tumor
GPR25	Type 1 T helper cell	Anti-tumor	KLRC1	Natural killer T cell	Anti-tumor
GREM2	Type 1 T helper cell	Anti-tumor	FUT4	Natural killer T cell	Anti-tumor
HAVCR1	Type 1 T helper cell	Anti-tumor	ICAM2	Natural killer T cell	Anti-tumor
HSD11B1	Type 1 T helper cell	Anti-tumor	IL32	Natural killer T cell	Anti-tumor
HUNK	Type 1 T helper cell	Anti-tumor	LAMP2	Natural killer T cell	Anti-tumor
IGF2	Type 1 T helper cell	Anti-tumor	LILRB5	Natural killer T cell	Anti-tumor
RCSD1	Type 1 T helper cell	Anti-tumor	KLRG1	Natural killer T cell	Anti-tumor
RYR1	Type 1 T helper cell	Anti-tumor	HSPA4	Natural killer T cell	Anti-tumor
SAV1	Type 1 T helper cell	Anti-tumor	HSPB6	Natural killer T cell	Anti-tumor
SELE	Type 1 T helper cell	Anti-tumor	ISM2	Natural killer T cell	Anti-tumor
SELP	Type 1 T helper cell	Anti-tumor	ITIH2	Natural killer T cell	Anti-tumor
SH3KBP1	Type 1 T helper cell	Anti-tumor	KDM4C	Natural killer T cell	Anti-tumor
SIT1	Type 1 T helper cell	Anti-tumor	KIR2DS4	Natural killer T cell	Anti-tumor
SLC35B3	Type 1 T helper cell	Anti-tumor	KIRREL3	Natural killer T cell	Anti-tumor
SIGLEC10	Type 1 T helper cell	Anti-tumor	SDCBP	Natural killer T cell	Anti-tumor
SKAP1	Type 1 T helper cell	Anti-tumor	NFATC2IP	Natural killer T cell	Anti-tumor
THUMPD2	Type 1 T helper cell	Anti-tumor	MICB	Natural killer T cell	Anti-tumor
TIGIT	Type 1 T helper cell	Anti-tumor	KIR2DL1	Natural killer T cell	Anti-tumor
ZEB2	Type 1 T helper cell	Anti-tumor	KIR2DL3	Natural killer T cell	Anti-tumor
ENC1	Type 1 T helper cell	Anti-tumor	KIR3DL1	Natural killer T cell	Anti-tumor
FAM134B	Type 1 T helper cell	Anti-tumor	KIR3DL2	Natural killer T cell	Anti-tumor
FBXO30	Type 1 T helper cell	Anti-tumor	NCR1	Natural killer T cell	Anti-tumor
FCGR2C	Type 1 T helper cell	Anti-tumor	FOSL1	Natural killer T cell	Anti-tumor
STAC	Type 1 T helper cell	Anti-tumor	TSLP	Natural killer T cell	Anti-tumor
LTC4S	Type 1 T helper cell	Anti-tumor	SLC7A7	Natural killer T cell	Anti-tumor
MAN1B1	Type 1 T helper cell	Anti-tumor	SPP1	Natural killer T cell	Anti-tumor
MDH1	Type 1 T helper cell	Anti-tumor	TREM2	Natural killer T cell	Anti-tumor
MMD	Type 1 T helper cell	Anti-tumor	UBASH3A	Natural killer T cell	Anti-tumor
RGS16	Type 1 T helper cell	Anti-tumor	YBX2	Natural killer T cell	Anti-tumor
IL12A	Type 1 T helper cell	Anti-tumor	CCDC88A	Natural killer T cell	Anti-tumor
P2RX5	Type 1 T helper cell	Anti-tumor	CLEC1A	Natural killer T cell	Anti-tumor
CD97	Type 1 T helper cell	Anti-tumor	THBD	Natural killer T cell	Anti-tumor
ITGB4	Type 1 T helper cell	Anti-tumor	PDPN	Natural killer T cell	Anti-tumor
ICAM3	Type 1 T helper cell	Anti-tumor	VCAM1	Natural killer T cell	Anti-tumor
METRNL	Type 1 T helper cell	Anti-tumor	EMR1	Natural killer T cell	Anti-tumor
TNFRSF1A	Type 1 T helper cell	Anti-tumor	CREB5	Neutrophil	Pro-tumor
IRF1	Type 1 T helper cell	Anti-tumor	CDA	Neutrophil	Pro-tumor
HTR2B	Type 1 T helper cell	Anti-tumor	CHST15	Neutrophil	Pro-tumor
CALD1	Type 1 T helper cell	Anti-tumor	S100A12	Neutrophil	Pro-tumor
MOCOS	Type 1 T helper cell	Anti-tumor	APOBEC3A	Neutrophil	Pro-tumor
TRAF3IP2	Type 1 T helper cell	Anti-tumor	CASP5	Neutrophil	Pro-tumor
TLR8	Type 1 T helper cell	Anti-tumor	MMP25	Neutrophil	Pro-tumor
TRAF1	Type 1 T helper cell	Anti-tumor	HAL	Neutrophil	Pro-tumor

DUSP14	Type 1 T helper cell	Anti-tumor	C1orf183	Neutrophil	Pro-tumor
IL17A	Type 17 T helper cell	Anti-tumor	FFAR2	Neutrophil	Pro-tumor
IL17RA	Type 17 T helper cell	Anti-tumor	MAK	Neutrophil	Pro-tumor
C2CD4A	Type 17 T helper cell	Anti-tumor	CXCR1	Neutrophil	Pro-tumor
C2CD4B	Type 17 T helper cell	Anti-tumor	STEAP4	Neutrophil	Pro-tumor
CA2	Type 17 T helper cell	Anti-tumor	MGAM	Neutrophil	Pro-tumor
CCDC65	Type 17 T helper cell	Anti-tumor	BTNL8	Neutrophil	Pro-tumor
CEACAM3	Type 17 T helper cell	Anti-tumor	CXCR2	Neutrophil	Pro-tumor
IL17C	Type 17 T helper cell	Anti-tumor	TNFRSF10C	Neutrophil	Pro-tumor
IL17F	Type 17 T helper cell	Anti-tumor	VNN3	Neutrophil	Pro-tumor
IL17RC	Type 17 T helper cell	Anti-tumor	ITGA2B	Plasmacytoid dendritic cell	Pro-tumor
IL17RE	Type 17 T helper cell	Anti-tumor	GABARAP	Plasmacytoid dendritic cell	Pro-tumor
IL23A	Type 17 T helper cell	Anti-tumor	GPX1	Plasmacytoid dendritic cell	Pro-tumor
ILDR1	Type 17 T helper cell	Anti-tumor	KRT23	Plasmacytoid dendritic cell	Pro-tumor
LONRF3	Type 17 T helper cell	Anti-tumor	PROK2	Plasmacytoid dendritic cell	Pro-tumor
SH2D6	Type 17 T helper cell	Anti-tumor	RALB	Plasmacytoid dendritic cell	Pro-tumor
TNIP2	Type 17 T helper cell	Anti-tumor	RETNLB	Plasmacytoid dendritic cell	Pro-tumor
ABCA1	Type 17 T helper cell	Anti-tumor	RNF141	Plasmacytoid dendritic cell	Pro-tumor
ABCB1	Type 17 T helper cell	Anti-tumor	SEC14L1	Plasmacytoid dendritic cell	Pro-tumor
ADAMTS12	Type 17 T helper cell	Anti-tumor	SEPX1	Plasmacytoid dendritic cell	Pro-tumor
ANK1	Type 17 T helper cell	Anti-tumor	EMP3	Plasmacytoid dendritic cell	Pro-tumor
ANKRD22	Type 17 T helper cell	Anti-tumor	CD300LF	Plasmacytoid dendritic cell	Pro-tumor
B3GALT2	Type 17 T helper cell	Anti-tumor	ABTB1	Plasmacytoid dendritic cell	Pro-tumor
CAMTA1	Type 17 T helper cell	Anti-tumor	KLHL21	Plasmacytoid dendritic cell	Pro-tumor
CCR9	Type 17 T helper cell	Anti-tumor	PHRF1	Plasmacytoid dendritic cell	Pro-tumor
CD40	Type 17 T helper cell	Anti-tumor			